Rational synthesis of polymer coated inorganic nanoparticles-MWCNT hybrids via solvophobic effects

Pablo Quijano Velasco [a,*], Vikram Karde [b], Yumiko Ito [a], Jerry Y.Y. Heng [b], Kyriakos Porfyrakis [c,*], Nicole Grobert [a,*]

[a] Department of Materials, University of Oxford, Parks Road, Oxford, OX1 3PH, UK
[b] Department of Chemical Engineering, Imperial College London, South Kensington Campus, London, SW7 2AZ, UK
[c] Faculty of Engineering and Science, University of Greenwich, Central Avenue, Kent, ME4 4TB, UK

ARTICLE INFO

ABSTRACT

The efficient synthesis of inorganic nanoparticle-carbon nanotube hybrids requires the development of models and synthetic guidelines that can be used to maximise the interactions between both nanomaterials. Herein we report the application of the Hansen surface energy based solubility parameter theory as a model for the selection of solvents that can maximise the interactions between iron oxide nanoparticles and MWCNTs. To achieve this, we synthesized iron oxide nanoparticle-MWCNT hybrid materials in three different solvents and characterized their composition with TGA. The solvent was found to have a significant impact in the final amount of iron oxide composition of the hybrids. The Hansen surface energy based solubility parameters of MWCNTs were characterized via inverse gas chromatography and were used to evaluate the interactions between the MWCNTs and the solvent media. Under this model we expected that large differences between the Hansen surface energy based solubility parameters of solvents and MWCNTs would be correlated with larger incorporation of iron oxide nanoparticles in the hybrids. The amount of iron oxide nanoparticles found in the hybrids were indeed consistent with the predictions of the Hansen surface energy based solubility parameter theory making it a powerful tool for the design of nanoparticle-carbon nanotube hybrids.

1. Introduction

Hierarchical nanostructures that incorporate different nanomaterials have demonstrated to display synergistic properties that arise from the close interaction between their constituents. Among the whole plethora of possible nanostructures, the synthesis of materials that incorporate nanoparticles and carbon nanotubes (CNTs) have been highlighted for their potential applications in energy storage [1,2], catalysis [3,4], optoelectronic [5], photovoltaic [6] and light emitting devices [7]. In addition, these material systems are particularly suitable for the controlled bottom-up synthesis of nanostructures through simple wet chemical methods due to the capability of nanoparticles to be dispersed in a wide range of

solvents by the stabilisation of surface ligands [8]. In this way the synthesis of hybrid structures can be obtained via the non-covalent interactions between the surface ligands of nanoparticles and CNTs. Most literature so far has focused on reporting particular synthesis methods and little attention has been given to studies that attempt to elucidate what are the parameters affecting the interactions between nanoparticles and CNTs. In order to fully exploit the potential of nanoparticle-carbon nanotube hybrids more studies should focus in proposing general guidelines for the rational synthesis of these hybrid structures.

In general, the interactions between nanoparticles that are stabilised by surface ligands and CNTs have been classified as electrostatic [9], hydrogen bond [10], $\pi - \pi$ interactions [11,12], Van der Waals [13], solvophobic [14] and charge transfer interactions [15]. Although this classification is useful to understand how the chemical composition of the nanoparticles might be driving the functionalization of CNTs, it does not provide practical guidelines of how these interactions might be maximised. Only a handful of studies have proposed models that can be used to predict the effect that some parameters have in the non-covalent synthesis

---

of nanoparticle-carbon nanotube hybrids. The limited literature in this topic have focused on the estimation of the interactions between CNT and the nanoparticle core [13,16]. In particular, Rance et al. [16] studied the synthesis of gold nanoparticles (AuNPs) and multiwall carbon nanotubes (MWCNTs) hybrids in different solvents. They found that the dielectric constant seemed to play a key role in the amount of nanoparticles incorporated into the hybrid. They hypothesised that the solvent served as a dielectric that regulated the inherent negative surface charge of both AuNP and MWCNTs. In this way, as the dielectric constant of the solvent decreased, the functionalization of MWCNTs with AuNPs increased due to an electrostatic effect.

Another way that solvents affect the interactions between CNTs and nanoparticles are through solvophobic effects. In this case, the driving force of the functionalization is the decrease of the high energy interphase between CNTs and solvent molecules due to the adsorption of nanoparticles on the CNT surface. However, there have been no models so far that could be used to estimate the unfavourable solvent-CNT interactions to predict the degree of functionalization of CNTs with inorganic nanoparticles in different solvents. Previously, we have reported that the Hansen Surface Energy Based Solubility Parameter (SEBSP) theory can be used to predict the degree of polymer functionalization of MWCNTs, which is driven by analogous solvophobic effects [17]. In particular, our previous research found that the Hansen SEBSP theory is the most suitable for the prediction of the degree of polystyrene functionalization of MWCNTs in different organic solvents [17].

The Hansen SEBSP theory is derived from the Hansen solubility parameter theory (HSP) and differs in the use of surface energy values (E_S) of substances instead of their cohesive energy. Thus, the Hansen SEBSP proposes that the total surface energy of a substance ($E_{S,Total}$) should be divided into dispersive, polar and electron exchange contributions as follows [18]:

$$E_{S,Total} = E_{S,D} + E_{S,P} + E_{S,H} \tag{1}$$

Each of these three contributions have a related solubility parameter ($\partial_{D,P,H}$) that is specific for each substance and defined as [18]:

$$\partial_{D,P,H} = \sqrt{E_{S,D,P,H}} \tag{2}$$

If the solubility parameters of two substances such as CNTs and solvents are plotted in a 3-dimensional space, the distance between each point will be proportional to their enthalpy of mixing. The Hansen SEBSP distance (R_a) is calculated as follows [18]:

$$R_a = \sqrt{\left(\partial_D^{CNT} - \partial_D^{Sol}\right)^2 + \left(\partial_P^{CNT} - \partial_P^{Sol}\right)^2 + \left(\partial_H^{CNT} - \partial_H^{Sol}\right)^2} \tag{3}$$

Where $\partial_{D,P,H}^{CNT}$ and $\partial_{D,P,H}^{sol}$ are the SEBSP of the CNTs and solvent respectively. Thus, the enthalpy of mixing is minimised when the SEBSP of substance are similar, which in turn leads to a small R_a distance. For the purpose of the functionalization of MWCNTs with nanoparticles through solvophobic effects, we would expect that as the R_a value between a solvent and the CNTs increases a higher number of nanoparticles would interact with the CNTs to minimise the unfavourable solvent-CNT interactions.

The values for the SEBSP of a substance can be directly calculated using previously reported surface energies and HSP that were originally derived using the cohesive energies of each substance [18]. While the values for the HSP of organic solvents are widely available in the literature, obtaining the specific values for nanomaterials such as CNTs is not as straight forward. So far, the HSP of CNTs have been reported by evaluating CNT dispersions in different solvents [18–20] and through inverse gas chromatography (IGC) [21]. Two conclusions can be drawn from these studies: First, the HSP seem to vary for different CNT samples with different degree of graphitization, number of walls and surface chemistry [19,20].

For this reason, it should be expected that variations will occur in samples that have been synthesized by different methodologies, which would present different structural characteristics and surface compositions. Second, the measurement of the HSP of CNTs through inverse gas chromatography has provided the best quality of prediction that can be found in the literature [21].

IGC estimates the HSP of a CNT sample by the direct measurement of the enthalpy of absorption of solvent probes on the surface of the CNTs. On the other hand, procedures based on dispersion methodologies are not directly measuring thermodynamic interactions but the stability of CNT dispersions in different solvents. Previous theoretical research has found that the stability of CNT dispersion not only depends on the solvent-CNT interactions but also the conformation of the solvation sphere and the surface charge of the CNTs [22]. For this reason, dispersion studies should not be considered as reliable in comparison to IGC to evaluate the solvent-CNT interactions.

Herein, we used the SEBSP to understand the difference of iron oxide nanoparticle (IONP) content observed in IONP-MWCNTs hybrids synthesized in different solvents. To achieve this, we synthesized IONPs coated with oleylamine ligands (OAIONPs) through a thermal decomposition method. To obtain a material that could be analogous to our previous research of polystyrene functionalization of MWCNTs, we exchanged the oleylamine surface ligands for short polystyrene chains thus obtaining polystyrene coated IONPs (PSIONPs). Afterwards we synthesized PSIONP-MWCNT hybrids in three different organic solvents and quantitatively characterized the content of iron oxide nanoparticles present in the hybrids. In addition, we measured the SEBSP of the MWCNTs through IGC and calculated the Hansen SEBSP distance with each solvent. Finally, the Hansen SEBSP distance was compared with the amount of PSIONPs found in the hybrids showing a strong correlation between them.

2. Experimental section

2.1. Materials

The MWCNTs used during this study were NC7000 MWCNTs obtained from Nanocyl.

For the IGC characterization of the MWCNTs the following solvents were used. n-Octane (anhydrous ≥99%), n-heptane (HPLC grade ≥99%), n-hexane (HPLC grade ≥99.5%), ethanol (puriss. p.a., ACS reagent, absolute alcohol), ethyl acetate (HPLC grade ≥99.7%), acetonitrile (HPLC grade ≥99.9%) and dichloromethane (HPLC grade ≥99.8%) were purchased from Sigma Aldrich. Toluene (≥99.5%, AnalaR NORMAPUR ACS, Reag. Ph. Eur.) was obtained from VWR chemicals.

Tetrahydrofuran (HPLC grade ≥99.9%), styrene (containing 4-Tertbutyl catechol ≥99%), 2,2-bipyridine (99%), 2-(4-bromomethyl)phenylpropionic acid (96%) and copper (I) bromide (99.999% trace metal basis) were used for the synthesis of polystyrene by atom transfer polymerisation and were purchased from Sigma-Aldrich.

The iron (III) acetylacetonate (≥99.9% trace metals basis), oleylamine (technical grade 70%), ethanol (puriss.), tetrahydrofuran (HPLC grade ≥99.9%), dichloromethane (DCM) (≥99.98%) and toluene (HPLC grade ≥ 99.99%) used for the nanoparticle synthesis, ligand exchange and nanoparticle functionalization of NC7000 MWCNTs were purchased from Sigma Aldrich.

2.2. General characterization

Transmission Electron Microscopy images were recorded on a JEOL 3000F TEM microscope operating in an accelerating voltage of 300 or 200 kV.

FTIR spectroscopy data was acquired in a Varian Excalibur FTS 3500 FTIR spectrometer using attenuated total reflection (ATR) mode.

Themogravimetric analysis was performed under air atmosphere in a Perkin Elmer Diamond TG/DTA6300. Approximately 5 mg of sample were used for each experiment. For the analysis of the NP-MWCNTs composites in air the samples were preheated from room temperature to 100 °C, where they were held in an isothermal scan for 10 min to remove water from the sample pan. The sample was heated at a rate of 10 °C/minute to 340 °C, where it was held in a isothermal scan for 20 min. Finally, the sample was heated to 800 °C at a rate of 10 °C/minute.

For X-ray photoelectron spectroscopy (XPS) analysis the spectrum was acquired using a Thermo Scientific K-Alpha XPS instrument equipped with a microfocused monochromated Al X-ray source.

2.3. IGC analysis of MWCNTs

The surface energy analysis of MWNCTs was performed using an inverse gas chromatography surface energy analyser (IGC SEA) manufactured by Surface Measurement Systems (SMS). For the analysis, approximately 10 mg of MWCNTs sample was packed into a silanised glass column (internal diameter of 3 mm) with silanised glass wool on both ends to prevent powder movement. The sample was packed by mechanical tapping using a jolting voltmeter (SMS) to remove voids in the sample. The packed column was placed in an oven to condition for analysis at a 0%RH (relative humidity) for 2 h under helium flow. The IGC measurements were performed in a range of temperature form 50–110 °C at 0%RH. Helium was used as carrier gas at a flow rate of 12 mL/min. Methane was used as a reference gas to determine the dead volume. The analysis was performed at an infinite dilution region using octane, heptane and hexane to determine the dispersive surface energy interactions of MWCNTs. To evaluate the non-dispersive hydrogen bonding interactions, ethyl acetate, dichloromethane, toluene and acetonitrile were employed as probe molecules.

2.4. Synthesis of iron oxide nanoparticles

The synthesis of iron oxide nanoparticles was conducted according previous research [23,24]. In a typical experiment iron (III) acetylacetonate (1g, 3mmol, 1eq) and 30 mL of oleylamine were measured and transferred to a 100 mL three-necked round bottom flask fitted with an immersion-type thermocouple. The flask was connected to Schlenk line and the thermocouple was connected to a proportional-integral-derivative (PID)-controlled heating mantle and the flask sealed with a ground-glass stopper. The mixture was evacuated under vacuum and flushed with nitrogen a total of three times. The mixture was heated under vacuum to 100 °C, the temperature was held for 30 min to remove any moisture from the reaction mixture. Afterwards, the mixture was heated to 300 °C and the temperature was held for 1 h. The reaction mixture was cooled to room temperature and 50 mL of ethanol were added. The mixture was transferred into 3 separate centrifuge tubes and the mixture was centrifuged at 4250 rpm for 10 min resulting in the separation of a clear supernatant and a black pellet in the bottom of the tubes. The clear supernatant was discarded, 10 mL of ethanol were added to each tube and the solid pellets were sonicated for 5 min. The mixture was centrifuged at 4250 rpm for 5 min, the clear supernatant was discarded and the nanoparticles were solubilised in an organic solvent.

2.5. Synthesis of polystyrene

The methodology for the synthesis of polystyrene was based on a ATRP procedure reported previously using (bromomethyl)phenyl]propionic acid as an initiator [25]. This specific initiator molecule incorporated a COOH end group that was used to coordinate the polystyrene with the IONPs. ^{1}H NMR was consistent with the expected polystyrene spectrum and MALDI-TOF mass spectrometry showed that the difference of the molecular mass between peaks is equal to 104 g/mol consistent with the expected mass of styrene monomers. ^{1}H NMR (450MHz, CDCl$_3$): 7.10-6.50 ppm (broad, aromatic H), 4.5-4.2 (duplet, CH$_2$-Br) 2.5-1.1 ppm (broad, CH+CH$_2$). The polymer number average molecular weight (Mn = 3333 g/mol) and weight average molecular weight (Mw = 3609) were determined by gel permeation chromatography.

2.6. Synthesis of polystyrene coated IONPs

In a typical experiment 5 mL of a 5 mg/mL solution of polystyrene in toluene, 1 mL of 25 mg/mL solution of oleylamine coated IONP and 4 mL of toluene were mixed and left stirring at room temperature for 24 h. The mixture was transferred to a centrifuge tube and precipitated by adding ethanol causing the aggregation of the nanoparticles. The mixture was centrifuged for 10 min at 4025 rpm, the supernatant was discarded and the solid pellet of IONPs was redispersed in 500 μL of toluene. To wash the unbound polystyrene from the sample, the nanoparticles were washed by adding 500 μL of ethanol, followed by centrifugation at for 10 min at 4025 rpm. The supernatant was discarded and the solid pellet of IONPs was redispersed in 500 μL of toluene and washed using the same procedure for a total of five repetitions. Finally, the nanoparticles were dried using a nitrogen air gun and dispersed in a desired organic solvent (DCM, THF or toluene).

2.7. Synthesis of IONP-MWCNT hybrids

A typical experiment for the non-covalent nanoparticle functionalization of MWCNTs with iron oxide nanoparticles consisted of mixing 5 mg of MWCNT, 1 mL of IONP solution in an organic solvent (DCM, Toluene or THF) with a concentration approximately 25 mg/mL and 4 ml of the corresponding solvent (Toluene, DCM or THF). The mixture was ultrasonicated for 1 h in order to disperse the MWCNTs in the solvent medium. Afterwards the mixture was vacuum filtered and washed 3 times with 10 mL of solvent. The solid filtrate was re-dispersed in 20 mL of solvent and ultrasonicated for 15 min, filtered and washed 3 times with 10 mL of solvent. This procedure was repeated three times in total.

3. Results and discussion

3.1. Synthesis of MWCNT-PSIONP hybrids

IONPs stabilised with oleylamine ligands (OAIONPs) were synthesized as described in the Experimental Section and were characterized by TEM. The TEM micrographs in Figure S1 show that the OAIONPs presented an average diameter of 7.7 ± 1.8nm. It can be seen that the OAIONPs are not forming large disordered agglomerates but are instead arranged in ordered hexagonal domains that are characteristic of ligand stabilised nanoparticles formed by the evaporation of stable nanoparticle dispersions [26]. DLS was used to characterise the stability of OAIONPS dispersions in DCM, toluene and THF. The results showed that the particles were well dispersed in all three organic solvents and presented a unimodal distribution of particle size with an average hydrodynamic diameter of approximately 10 nm. By subtracting the core diameter obtained via TEM from the DLS hydrodynamic diameter we calculated that the oleylamine surface ligands are extending into the bulk of the solution with a ligand height of approximately 2.3 nm (see Figure S3).
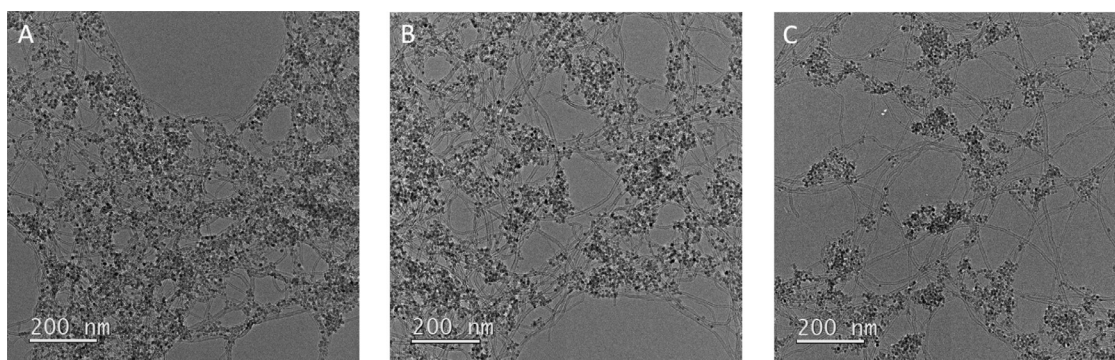
Fig. 1. PSIONP-MWCNT hybrids synthesized in A) THF B) Toluene C) DCM. The PSIONPS are found in close contact with the surface of the MWCNTs. There was no individual PSIONPS found in areas where MWCNTs were not present, suggesting that the PSIONP in the hybrids are in fact interacting with the MWCNTs instead of separating into a different phase. It can be also observed that the amount of PSIONP found in the hybrids is dependent on the solvent used during the functionalization. In this case the hybrids synthesized in THF seemed to present the larger content of PSIONPs, while the hybrids synthesized in DCM presented the least amount of PSIONPs.

A ligand exchange procedure was used to exchange the oleylamine surface coating with short polystyrene chains. The procedure involved mixing the OAIONPs with polystyrene molecules synthesized via ATRP that presented carboxylic acid end-groups. The weakly bound oleylamine was displaced by the polystyrene molecules due to a more robust coordination bond between the carboxylate end-group and the iron atoms at the surface of the particle [27]. The PSIONPs were found to form stable dispersions in DCM, toluene and THF. The TEM micrographs of the samples showed no visible disordered aggregation of the particles in any of the solvents and presented similar ordered domains as was observed for the OAIONPs (see Figure S2).The stability of the PSIONP dispersions was confirmed by DLS characterization, which showed a unimodal distribution with an average hydrodynamic diameter between 12.3–13.3 nm in all three solvents (see Figure S3). The resulting height of the surfactant layer after ligand exchange was between 4.6-5.6 nm for the PSIONPs, which is much larger in comparison to the height observed for OAIONPs. The increased hydrodynamic diameter observed after the ligand exchange strongly suggests that the IONPs have exchanged a smaller surface ligand such as oleylamine for a longer ligand such as our short polystyrene chains. These observations are consistent with previous reports where IONPs and gold nanoparticles coated with oleic acid and oleylamine were exchanged with short polystyrene chain ligands [28].

FTIR analysis before and after the ligand exchange procedure demonstrates the successful displacement of oleylamine ligands with polystyrene. In Figure S4 it can be observed that the FTIR spectrum significantly changed after the ligand exchange procedure. This remark is more evident in Figure S4B,D and F, where it can be observed that after the ligand exchange procedure there is the presence of characteristic polystyrene signals such as the C-H aromatic stretch peaks in the range between 3000–3100 cm^{-1}, three aromatic C= C stretch signals in the range between 1450–1600 cm^{-1}, and the C-H aromatic out-of-plane bending peaks in the range between 675–900 cm^{-1}.

The synthesis of PSIONP-MWCNT hybrids was performed using THF, toluene and dichloromethane as solvent medium. These solvents were selected in order to obtain a representative sample of molecules with different physicochemical properties that could interact through different intermolecular forces with the MWCNTs and PSIONPs. According to this selection, toluene represents solvents with a non-polar character. THF represents solvents with a dipole constant that show hydrogen bonding and electron donor characteristics. Finally, DCM represents solvents with dipole constant that have no hydrogen bonding or electron donating character. Thus, we could compare the effect that solvents with dif-

ferent properties have in the final composition of the synthesized PSIONP-MWCNT hybrids. The functionalization of MWCNTs with PSIONPs was performed by mixing under ultrasonication a solution of PSIONPs and MWCNTs in a 5:1 wt ratio. The PSIONP-MWCNT hybrids were filtered, redispersed in the same solvent used during the functionalization and ultrasonicated. This washing procedure was repeated three times. After the third wash the characteristic amber colour of PSIONPs in the liquid phase separated by filtration disappeared completely, suggesting that most free PSIONPs had been washed away from the solid phase.

The TEM characterization of the hybrids synthesized in all three different solvents are presented in Fig. 1. The TEM characterization showed that the PSIONPs are coating and forming aggregates around the MWCNTs, while no evidence was found of individual or aggregated PSIONPs in areas separated from the MWCNTs. Thus, we can conclude that the PSIONPs are in fact functionalizing the MWCNT walls and not segregating into a different phase. In addition, it can be observed that the amount of PSIONPs functionalizing the surface of the MWCNTs seems to be dependent on the solvent used during synthesis. The PSIONP-MWCNT hybrids that seemed to present a larger amount of nanoparticles in their structure were synthesized in THF (Fig. 1A) followed by the hybrids made in toluene (Fig. 1B) and finally DCM (Fig. 1C).

The PSIONP-MWCNT hybrids were dried and analysed in TGA to obtain the composition of each hybrid. The analysis of the samples was performed under air atmosphere with two heating profiles that aimed to decouple the oxidation of the organic ligands and the MWCNTs. Figure 2 show an example of the TGA time profile used for the analysis of the PSIONPs-MWCNTs hybrids. As it can be observed in Figure 2B, we first performed a heating scan from 100 to 340 °C a temperature at which the polystyrene chains started to decompose. Afterwards the temperature was held constant at 340 °C for 20 min to fully decompose the PS ligands present in the sample. Finally, a second heating step from 340 to 800 °C was used to oxidize the remaining MWCNTs. The determination of the weight content of ligands, MWCNTs and iron oxide in the samples is better described in Fig. 2A. The first observed weight loss corresponds to the polystyrene ligands coating the PSIONPs, the second weight loss correspond to the MWCNT content in the sample and the remaining weight correspond to the weight percentage of iron oxide. The determination of the composition of the PSIONP-MWCNT hybrids through this heating profile is consistent with the temperature of decomposition observed in the TGA curves for the individual analysis of polystyrene, PSIONPs and MWCNTs that are presented in Figure S5.

The summary of the TGA results is presented in Table 1. The TGA analysis provided us a detailed examination of the compo-

Table 1
Summary of the composition of the PSIONP-MWCNT hybrids calculated by TGA.

Solvent	Average polystyrene weight [wt%]	Average MWCNT weight [wt%]	Average iron oxide weight [wt%]	Average IONP weight [wt%]	Average IO:MWCNT ratio	Average IONP: MWCNT ratio
THF	8.9 ± 0.3	17.8 ± 2.0	71.5 ± 2.4	80.4 ± 2.45	4.1 ± 0.6	4.6 ± 0.6
Toluene	14.1 ± 1.5	25.5 ± 1.3	57.8 ± 1.5	71.9 ± 1.4	2.3 ± 0.2	2.8 ± 0.2
DCM	13.8 ± 0.2	28.3 ± 2.3	55.1 ± 2.7	68.9 ± 2.6	2.0 ± 0.3	2.5 ± 0.3
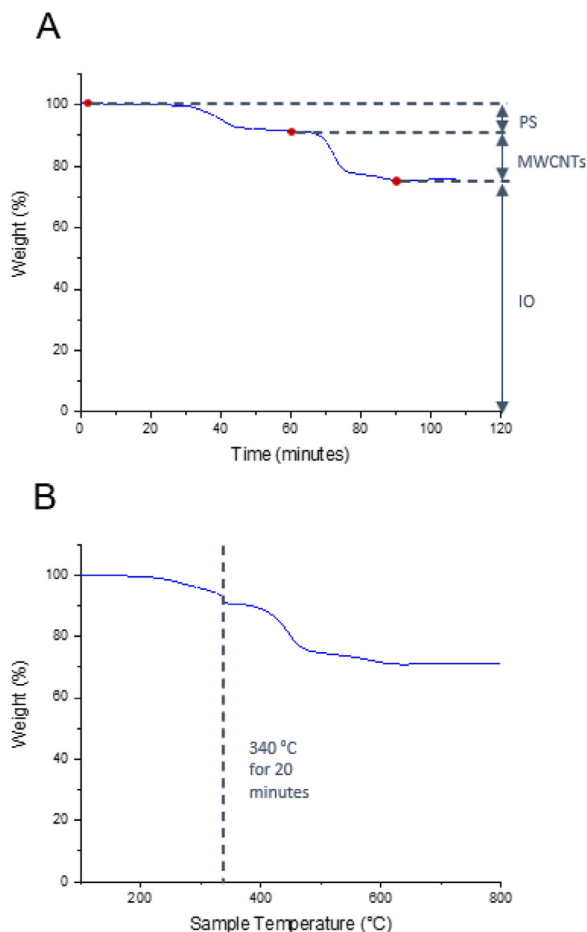
Fig. 2. TGA analysis of the samples A)PSIONPs-MWCNTs TGA time profile. An isothermal scan at 340 °C was used to fully decompose the polystyrene ligands B) PSIONPs-MWCNTs TGA temperature profile. The first weight loss is attributed to the oxidation of polystyrene ligands and the second weight loss is attributed to the oxidation of MWCNTs.

sition of ligands, MWCNTs and iron oxide (IO) content of the PSIONP-MWCNTs hybrids. In addition to the values directly obtained from the TGA profiles, we estimated the PSIONP weight composition in the samples by adding the weight percentage composition of polystyrene and iron oxide. It can be observed from Table 1 that the overall weight percentage composition of the PSIONP varied greatly across the PSIONP-MWCNT samples depending on the solvent used during the functionalization. Based on these observations we can appreciate that THF was the solvent that presented the largest proportion of PSIONPs, followed by toluene and DCM. These results show that there is a strong dependency between the solvent medium used during the synthesis and the amount of PSIONPs found in the hybrids. Moreover, the relatively small standard deviation (i.e. <20%) observed in the experiments strongly indicates that the synthesis in each solvent medium has a

characteristic degree of functionalization and is not due to random variation.

To obtain a more accurate value to be used for the comparison across the samples we calculated the iron oxide to MWCNT ratio (IO:MWCNT) and the PSIONP to MWCNT ratio (IONP:MWCNT). These values were computed by dividing the weight percentage composition of iron oxide or PSIONPs by the weight percentage composition of MWCNTs respectively. Using the weight ratios as comparison between samples helps to understand how the content of PSIONPs in relation with the MWCNT content varied across the experiments. As it can be observed the ratios varied in the order specified before where THF resulted as the solvent with a larger amount of PSIONP followed by toluene and DCM. With these metrics we can appreciate the extent of the increase in the PSIONP content between the samples, which was almost two-fold in THF when compared to DCM. This observation shows the important role that solvents can have to maximise the interactions between MWCNTs and nanoparticles for the synthesis of PSIONP-MWCNT hybrids.

Our previous research in the synthesis of functionalized MWCNTs with polystyrene through solvophobic effects, showed that the strength of the solvophobic interactions between solvents and MWCNTs can be estimated through the SEBSP theory. In addition, this model was shown to correlate with the differences of the amount of polystyrene functionalization of MWCNTs observed when they where prepared in different solvents [17]. To understand if the same solvophobic effects can explain the difference in the degree of PSIONP functionalization of MWCNTs in these three different solvents we first measured the HSP of MWCNTs using IGC.

3.2. IGC characterization of MWCNTs

Previous research has shown that the values of the HSP for CNTs samples can vary depending on their physical and chemical structure [19,20], for this reason we measured the surface energy and HSP of the MWNCTs used during this study to obtain the most accurate values for our analysis. The measurement of the HSP of MWCNTs was done through IGC characterization (see Section S5 for the summary of the experimental IGC data) using the Voelkel procedure [21,29]. Briefly, the enthalpy of adsorption (ΔH_{ads}) of 8 solvent probes were obtained by measuring the retention volume (V_g) of each probe at different temperatures. The ΔH_{ads} for each probe is calculated by obtaining the slope of the following linear relationship between V_g and the inverse of temperature (T):

$$In(V_g) = -\frac{\Delta H_{ads}}{RT} + C \tag{4}$$

The V_g of eight solvent probes where thus obtained from IGC analysis at temperatures ranging from 50 to 100 °C to calculate the ΔH_{ads} of each solvent on the MWCNTs. The ΔH_{ads} was then used to obtain the HSP of the MWCNTs by applying a multilinear regression on the following equation:

$$-\Delta H_{ads} = -\Delta E_{ads} = V_i(\delta_D^{sol}\delta_D^{CNT} + \delta_P^{sol}\delta_P^{CNT} + \delta_H^{sol}\delta_H^{CNT}) \tag{5}$$

Table 2
Values of the HSP for MWCNTs obtained through IGC.

Sample	Method	δ_d [MPa$^{1/2}$]	δ_p [MPa$^{1/2}$]	δ_h [MPa$^{1/2}$]	b	R^2	Ref
NC7000	Method 1	29.4	19.1	11.3	21.7	0.67	This work
NC7000	Method 2	20.5	6.7	7.2	-1.6	0.82	This work
CM250	-	21.3	6.8	3.2	-	-	[21]

Where V_i is the molar volume of the solvent molecules, $\delta_{D,P,H}^{sol}$ are the corresponding HSP of the solvent probes and $\delta_{D,P,H}^{CNT}$ are the HSP of the MWCNTs. The values for $\delta_{D,P,H}^{sol}$ and the V_i of the solvents are known quantities and were taken from previously reported values. The values for ΔH_{ads} have been obtained through IGC. Thus the linear equation presents 3 unknown coefficients that correspond to the $\delta_{d,p,h}^{CNT}$ of the MWCNTs, which can be obtained through a multilinear regression analysis [29].

Two different methods were used to estimate the HSP parameters of the MWCNTs and the results are presented in Table 2. In Method 1, we used the data directly obtained from the IGC for the multiple linear regression analysis. As it can be observed in Table 2, the results differ significantly from what it was obtained in previous reports. In particular, it is important to notice that the prediction given by the multiple linear regression has a large y-intercept value (b). It can be seen from Eq. (5) that an ΔH_{ads} equal to zero would be expected if the solvent probe presented a $\partial_{D,P,H}$ equal to zero. The observation of a large value for the y-intercept is not consistent with the theory since it would imply that a substance with $\delta_{D,P,H}$ equal to zero would still cause a change in the ΔH_{ads}. In Method 2, we added a hypothetical data point where a substance with a $\delta_{D,P,H}$ equal zero in order to correct for the observation of a large y-intercept.

With this consideration in place, we performed a multiple linear regression to obtain the HSP values of the MWCNTs. The result is presented in Table 2, it can be seen that the Method 2 used to calculate the HSP parameters of the MWCNTs resulted in values closer to the values reported previously for MWCNTs by Lim et al. [21]. The MWCNTs used for this study presented a larger δ_h in comparison to Lim et al. report, this difference can be explained by noting that the XPS analysis of the MWCNTs showed a 1.61% content of oxygen atoms while the sample used by Lim et al. presented 0.7% of oxygen atoms [21]. This difference suggests that the MWCNTs analysed in this study have larger amount of oxygen rich functional groups that can interact through hydrogen bonding interactions. On the other hand, the δ_h obtained through Method 1 is much larger to what it was reported previously for MWCNTs and does not correlate as closely with the increase of oxygen content determined by XPS characterization of our MWCNT sample and what was reported by Lim et al. This observations provide further support for including the hypothetical corrective point. Moreover, the value of the y-intercept was considerably closer to zero and the R^2 value of the linear regression was closer to 1, indicating that a higher degree of linear relationship is observed in comparison to the values obtained through Method 1. For these reasons the HSP values obtained through Method 2 were used for the calculation of the SEBSP of our MWCNTs.

The determination of the surface energy of the MWCNTs was obtained through IGC analysis according to the Schultz method [30]. The calculated dispersive surface energy was 116.6 mJ/m^2 at 50 °C, this value is similar to previous reports that have measured the surface energy of Nanocyl NC7000 MWCNTs. The polar contribution of the surface energy was determined to be 2.5 mJ/m^2. The total surface energy was calculated to be 119.1 mJ/m^2 by adding the polar and dispersive contribution of the surface energy, which

was used to obtain the SEBSP of the MWCNTs. The values of the HSP and total surface energy obtained through IGC were used to calculate the SEBSP of MWCNTs as described in Section S6 of the Supplementary Material. The analysis determined that the SEBSP of MWCNTs were $\partial_d = 10.2$ mJ$^{1/2}$/m, $\partial_p = 2.6$ mJ$^{1/2}$/m and $\partial_h = 2.8$ mJ$^{1/2}$/m.

The strong dependence that the solvent medium has on the functionalization of MWCNTs with the PSIONPS strongly suggest that solvophobic effects play an important role mediating the interactions between these nanomaterials. The strength of the solvophobic effects is related to the thermodynamics of the solvent-MWCNTs interactions. We propose that the estimation of the solvent-MWCNT interactions can also be used to understand the difference in the final composition of the PSIONP-MWCNT hybrids synthesized in different solvents. For this purpose we used the Hansen SEBSP theory to estimate the solvent-MWCNTs by calculating the R_a distance between each solvent and the MWCNTs according to Eq. (3). In this way, we would expect that as the R_a distance between the solvent and the MWCNTs increased the larger amount of PSIONPs should be found in the hybrids. In Fig. 3A we present the plot of the IO:MWCNT weight ratio obtained for the hybrids in the three different solvents against the Hansen SEBSP R_a distance between the MWCNTs and each solvent. It can be observed that for the PSIONPs-MWCNTs hybrids the amount of IONPs in the hybrid increased linearly when the Hansen SEBSP R_a distance increased. In addition, the order of the magnitude of the R_a distance was the same as the order observed for the IO:MWCNT ratio obtained from the experimental data. This positive correlation is consistent with our hypothesis and with the behaviour observed for the functionalization of MWCNTs with polystyrene [17]. This evidence supports the use of the SEBSP as a model to select solvents that maximise the content of nanoparticles for the synthesis of nanoparticle-MWCNT hybrids.

Finally, in Fig. 3B the values of the IO:MWCNT ratio was plotted against values of the dielectric constant of the solvents used during the synthesis. Rance et al. [16] previously demonstrated that the dielectric constant of the solvent may have an impact in the final composition of AuNP-MWCNT hybrids. In their study the difference in the amount of functionalization of MWCNTs with AuNPs was linked to the increase of localised negative surface charge in the nanomaterials when the dielectric constant of the solvent increased. However, in this case the dielectric constant of the solvent seems to have no correlation with the amount of nanoparticles found in the hybrid. On the other hand, the SEBSP seems to provide a more accurate descriptive model in this instance. While this observation does not discredit the observations reported by Rance et al. [16] it does suggest that the surface charge of the MWCNTs and the PSIONP do not play a crucial role in the final composition of these hybrids. Is important to note that the dodecanethiol ligands stabilising the gold nanoparticles in Rance et al. study are shorter in length in comparison to the polystyrene ligands used in our experiments. The electrostatic forces decrease quadratically with distance, which would explain why these forces might play a less important role in our system that uses larger polystyrene chains as surfactants coating the inorganic nanoparticles.

A

B
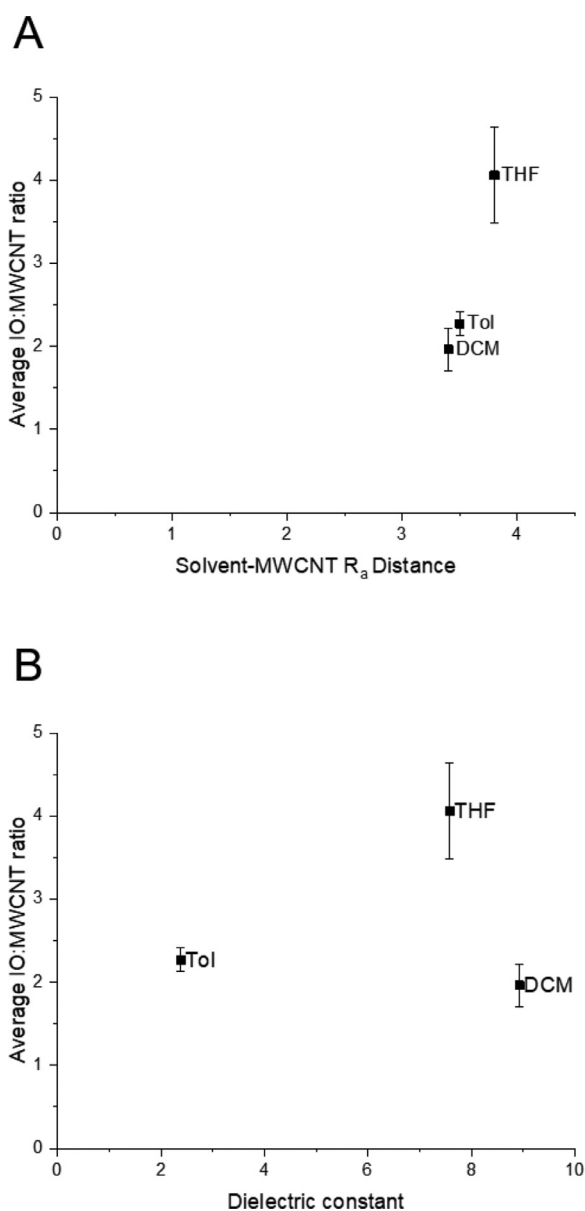
Fig. 3. Plot of the A) Hansen SEBSP difference between solvents and MWCNTs against IO:MWCNT ratio for PSIONPs-MWCNT B) Dielectric constant against the IO:MWCNT ratio for PSIONP-MWCNT.

4. Conclusions

In this work, we propose the use of the Hansen surface energy-based solubility parameter theory as a model to evaluate the amount of nanoparticle functionalization observed for MWCNTs in different solvents. In order to test this model we synthesized PSIONP-MWCNT hybrid materials in different solvents. The TGA analysis of the hybrids showed a characteristic nanoparticle composition depending on the solvent used during synthesis demonstrating the importance of the MWCNT-solvent interactions for the synthesis of PSIONP-MWCNT hybrids. To obtain the most accurate predictions from the Hansen SEBSP model we measured the surface properties of the MWCNTs with IGC obtaining the surface energy and Hansen solubility parameters of the material. With this data we calculated the SEBSP Hansen R_a distance between the MWCNTs and the solvents to understand the observed differences of composition of the PSIONP-MWCNT hybrids. The model showed good agreement with the experimental characterization, demon-

strating the important role that solvophobic interactions have during the functionalization of MWNCTs with inorganic nanoparticles. The large differences observed in the final composition of the PSIONP-MWCNT synthesized in different solvents were significant and the selection of an appropriate solvent can be used to maximise the nanoparticle-MWCNT interactions. These observations are relevant for applications where a large amount of nanoparticles are desired in the final composition of the nanoparticle-MWCNT hybrids. This fundamental study advances our current understanding of the synthesis of inorganic nanoparticle-MWCNT hybrids and we believe that will aid future research by providing synthetic guidelines for the synthesis of these hybrid materials.

Declaration of Competing Interest

The authors declare that they have no known competing financial interests or personal relationships that could have appeared to influence the work reported in this paper.

Appendix A. Supplementary material

The following data is provided as Supplementary Material for this article: TEM, DLS and FTIR characterisation of iron oxide nanoparticles (Section S1-S3). Supporting TGA characterisation of materials (Section S4). IGC characterisation data (Section S5). Details on calculation of surface energy based solubility parameters of MWCNTs and solvents (Section S6).

Supplementary material

Supplementary material associated with this article can be found, in the online version, at 10.1016/j.cartre.2021.100141.

References

[1] H. Wang, H. Dai, Strongly coupled inorganicnano-carbon hybrid materials for energy storage, Chem. Soc. Rev. 42 (7) (2013) 3088, doi:10.1039/c2cs35307e.

[2] J. Tuček, K.C. Kemp, K.S. Kim, R. Zboil, Iron-oxide-supported nanocarbon in lithium-ion batteries, medical, catalytic, and environmental applications, ACS Nano 8 (8) (2014) 7571–7612, doi:10.1021/nn501836x.

[3] Y. Liang, Y. Li, H. Wang, H. Dai, Strongly coupled inorganic/nanocarbon hybrid materials for advanced electrocatalysis, J. Am. Chem. Soc. 135 (6) (2013) 2013–2036, doi:10.1021/ja3089923.

[4] B. Wu, Y. Kuang, X. Zhang, J. Chen, Noble metal nanoparticles/carbon nanotubes nanohybrids: synthesis and applications, Nano Today 6 (1) (2011) 75–90, doi:10.1016/j.nantod.2010.12.008.

[5] Y. Kang, D. Kim, Enhanced optical sensing by carbon nanotube functionalized with CdS particles, Sens. Actuators A 125 (2) (2006) 114–117, doi:10.1016/j.sna.2005.06.021.

[6] X. Li, Y. Jia, J. Wei, H. Zhu, K. Wang, D. Wu, A. Cao, Solar cells and light sensors based on nanoparticle-grafted carbon nanotube films, ACS Nano 4 (4) (2010) 2142–2148, doi:10.1021/nn901563y.

[7] X. Li, Y. Jia, A. Cao, Tailored single-walled carbon nanotube–CdS nanoparticle hybrids for tunable optoelectronic devices, ACS Nano 4 (1) (2010) 506–512, doi:10.1021/nn901757s.

[8] G.A. Rance, A.N. Khlobystov, Interactions between nanoparticles and carbon nanotubes: directing the self-assembly of one-dimensional superstructures, in: Comprehensive Nanoscience and Nanotechnology, vol. 1–5, Elsevier, 2019, pp. 219–236.

[9] T. Sainsbury, D. Fitzmaurice, Carbon-nanotube-templated and pseudorotaxane-formation-driven gold nanowire self-assembly, Chem. Mater. 16 (11) (2004) 2174–2179, doi:10.1021/cm035368k.

[10] L. Han, W. Wu, F.L. Kirk, J. Luo, M.M. Maye, N.N. Kariuki, Y. Lin, C. Wang, C.-J. Zhong, A direct route toward assembly of nanoparticlecarbon nanotube composite materials, Langmuir 20 (14) (2004) 6019–6025, doi:10.1021/la0497907.

[11] L. Wang, J. Han, J. Hoy, F. Hu, H. Liu, M.M. Gentleman, M.Y. Sfeir, J.A. Misewich, S.S. Wong, Probing differential optical and coverage behavior in nanotube nanocrystal heterostructures synthesized by covalent versus non-covalent approaches, Dalton Trans. 43 (20) (2014) 7480, doi:10.1039/c3dt53405g.

[12] V. Georgakilas, V. Tzitzios, D. Gournis, D. Petridis, Attachment of magnetic nanoparticles on carbon nanotubes and their soluble derivatives, Chem. Mater. 17 (7) (2005) 1613–1617, doi:10.1021/cm0483590.

[13] T. Sainsbury, J. Stolarczyk, D. Fitzmaurice, An experimental and theoretical study of the self-assembly of gold nanoparticles at the surface of functionalized multiwalled carbon nanotubes, J Phys Chem B 109 (34) (2005) 16310–16325, doi:10.1021/jp051224c.

[14] A.V. Ellis, K. Vijayamohanan, R. Goswami, N. Chakrapani, L.S. Ramanathan, P.M. Ajayan, G. Ramanath, Hydrophobic anchoring of monolayer-protected gold nanoclusters to carbon nanotubes, Nano Lett. 3 (3) (2003) 279–282, doi:10.1021/nl025824o. https://pubs.acs.org/doi/10.1021/nl025824o

[15] G.A. Rahman, D.M. Guldi, E. Zambon, L. Pasquato, N. Tagmatarchis, M. Prato, Dispersable carbon nanotube/gold nanohybrids: evidence for strong electronic interactions, Small 1 (5) (2005) 527–530, doi:10.1002/smll.200400146.

[16] G.A. Rance, A.N. Khlobystov, Interactions of carbon nanotubes and gold nanoparticles: the effects of solvent dielectric constant and temperature on controlled assembly of superstructures, Dalton Trans. 43 (20) (2014) 7400, doi:10.1039/c3dt53372g.

[17] P. Quijano Velasco, K. Porfyrakis, N. Grobert, The application of the surface energy based solubility parameter theory for the rational design of polymer-functionalized MWCNTs, PCCP 21 (10) (2019) 5331–5334, doi:10.1039/C8CP07411A.

[18] S.D. Bergin, Z. Sun, D. Rickard, P.V. Streich, J.P. Hamilton, J.N. Coleman, Multicomponent solubility parameters for single-walled carbon nanotube solvent mixtures, ACS Nano 3 (8) (2009) 2340–2350, doi:10.1021/nn900493u.

[19] S. Detriche, G. Zorzini, J.-F. Colomer, A. Fonseca, J.B. Nagy, Application of the Hansen solubility parameters theory to carbon nanotubes, J. Nanosci. Nanotechnol. 8 (11) (2008) 6082–6092, doi:10.1166/jnn.2008.SW16.

[20] S. Detriche, J.B. Nagy, Z. Mekhalif, J. Delhalle, Surface state of carbon nanotubes and Hansen solubility parameters, J. Nanosci. Nanotechnol. 9 (10) (2009) 6015–6025, doi:10.1166/jnn.2009.1568.

[21] H.J. Lim, K. Lee, Y.S. Cho, Y.S. Kim, T. Kim, C.R. Park, Experimental consideration of the Hansen solubility parameters of as-produced multi-walled carbon nanotubes by inverse gas chromatography, PCCP 16 (33) (2014) 17466, doi:10.1039/C4CP02319F.

[22] A. Hardy, H. Bock, Toward high-throughput computational screening of carbon nanotube solvents, Langmuir 33 (43) (2017) 12267–12275, doi:10.1021/acs.langmuir.7b02600.

[23] D. Piché, I. Tavernaro, J. Fleddermann, J.G. Lozano, A. Varambhia, M.L. Maguire, M. Koch, T. Ukai, A.J. Hernández Rodríguez, L. Jones, F. Dillon, I. Reyes Molina, M. Mitzutani, E.R. González Dalmau, T. Maekawa, P.D. Nellist, A. Kraegeloh, N. Grobert, Targeted T1 magnetic resonance imaging contrast enhancement with extraordinarily small CoFe2O4 nanoparticles, ACS Appl. Mater. Interfaces 11 (7) (2019) 6724–6740, doi:10.1021/acsami.8b17162.

[24] Z. Xu, C. Shen, Y. Hou, H. Gao, S. Sun, Oleylamine as both reducing agent and stabilizer in a facile synthesis of magnetite nanoparticles, Chem. Mater. 21 (9) (2009) 1778–1780, doi:10.1021/cm802978z.

[25] P.Y. Keng, I. Shim, B.D. Korth, J.F. Douglas, J. Pyun, Synthesis and self-assembly of polymer-coated ferromagnetic nanoparticles, ACS Nano 1 (4) (2007) 279–292, doi:10.1021/nn7001213.

[26] C.B. Murray, C.R. Kagan, M.G. Bawendi, Synthesis and characterization of monodisperse nanocrystals and close-packed nanocrystal assemblies, Annu. Rev. Mater. Sci. 30 (1) (2000) 545–610, doi:10.1146/annurev.matsci.30.1.545.

[27] R.A. Harris, P.M. Shumbula, H. van der Walt, Analysis of the interaction of surfactants oleic acid and oleylamine with iron oxide nanoparticles through molecular mechanics modeling, Langmuir 31 (13) (2015) 3934–3943, doi:10.1021/acs.langmuir.5b00671.

[28] X. Ye, C. Zhu, P. Ercius, S.N. Raja, B. He, M.R. Jones, M.R. Hauwiller, Y. Liu, T. Xu, A.P. Alivisatos, Structural diversity in binary superlattices self-assembled from polymer-grafted nanocrystals, Nat. Commun. 6 (1) (2015) 10052, doi:10.1038/ncomms10052.

[29] A. Voelkel, K. Adamska, B. Strzemiecka, K. Batko, Determination of Hansen solubility parameters of solid materials by inverse gas-solid chromatography, Acta Chromatogr. 20 (1) (2008) 1–14, doi:10.1556/AChrom.20.2008.1.1.

[30] J. Schultz, L. Lavielle, C. Martin, The role of the interface in carbon fibre-epoxy composites, J. Adhes. 23 (1) (1987) 45–60, doi:10.1080/00218468708080469.